RESEARCH ARTICLE OPEN ACCESS

Intrathecal Inflammatory Profile and Gray Matter Damage Predict Progression Independent of Relapse Activity in Early Multiple Sclerosis

Damiano Marastoni,[1,*] Elisa Colato,[1,2,3,†] Matteo Foschi,[4,5,†] Agnese Tamanti,[1,†] Stefano Ziccardi,[1] Chiara Eccher,[1] Francesco Crescenzo,[1] Albulena Bajrami,[1] Gian Marco Schiavi,[1] Valentina Camera,[1] Daniela Anni,[1] Federica Virla,[1] Maddalena Guandalini,[1] Ermanna Turano,[1] Francesca Benedetta Pizzini,[6] Stefania Montemezzi,[7] Bruno Bonetti,[8] Owain Howell,[9] Roberta Magliozzi,[1,10] Richard S. Nicholas,[10] Antonio Scalfari,[10] Cristina Granziera,[11] Ludwig Kappos,[11] and Massimiliano Calabrese[1,*]

Correspondence
Dr. Marastoni
damiano.marastoni@univr.it
or Dr. Calabrese
massimiliano.calabrese@univr.it

Neurol Neuroimmunol Neuroinflamm 2025;12:e200399. doi:10.1212/NXI.0000000000200399

Abstract

Background and Objectives

The objective of this study was to determine, at the time of diagnosis, a CSF and MRI profile of intrathecal compartmentalized inflammation predictive of progression independent of relapse activity (PIRA) in early relapsing-remitting multiple sclerosis (RRMS).

Methods

This five-year prospective study included 80 treatment-naïve patients with RRMS enrolled at time of diagnosis. All patients underwent a lumbar puncture, regular neurologic evaluations including an Expanded Disability Status Scale (EDSS) assessment every 6 months, and an annual 3T brain MRI. PIRA was defined as having a confirmed disability progression independent of relapse activity. CSF levels of 68 inflammatory molecules were evaluated in combination with white matter and cortical lesion number (CLn) and volume, and regional gray matter thickness and volume.

Results

During the follow-up, 23 patients with RRMS (28.8%) experienced PIRA. At diagnosis, participants with PIRA were older (44.0 ± 10.7 vs 37.4 ± 12.4, $p = 0.017$) and with more disability (median EDSS score [interquartile range] of 3 [range 2–4] for PIRA vs 1.5 [range 1–2] for no PIRA group, $p < 0.001$). Random forest selected LIGHT, CXCL13, sTNFR1, sTNFR2, CCL7, MIF, sIL6Rbeta, IL35, CCL2, and IFNβ as the CSF markers best associated with PIRA. sTNFR1 (hazard ratio [HR] 10.11 [2.61–39.10], $p = 0.001$), sTNFR2 (HR 5.05 [1.63–15.64], $p = 0.005$), and LIGHT (HR 1.79 [1.11–2.88], $p = 0.018$) were predictors of PIRA at regression analysis. Baseline thalamus volume (HR 0.98 [0.97–0.99], $p = 0.005$), middle frontal gyrus thickness (HR 0.05 [0.01–0.72], $p = 0.028$), and CLn (HR 1.15 [1.05–1.25], $p = 0.003$) were MRI predictors of PIRA.

Discussion

A specific intrathecal inflammatory profile associated with TNF superfamily markers, CLn, and atrophy of several cortical and deep gray matter regions, assessed at time of diagnosis, is predictive of PIRA in early MS.

MORE ONLINE

Supplementary Material

*These authors contributed equally to this work as co-corresponding authors.

†These authors contributed equally to this work.

[1]Neurology B, Department of Neurosciences, University of Verona, Italy; [2]MS Centre, Department of Anatomy and Neuroscience, Amsterdam UMC, location VUmc, the Netherlands; [3]NMR Research Unit, Queen Square Multiple Sclerosis Centre, Department of Neuroinflammation, UCL Queen Square Institute of Neurology, Faculty of Brain Sciences, University College London, United Kingdom; [4]Department of Neuroscience, Multiple Sclerosis Center, Neurology Unit, S.Maria delle Croci Hospital, AUSL Romagna, Ravenna, Italy; [5]Department of Biotechnological and Applied Clinical Sciences, University of L'Aquila, Italy; [6]Department of Engineering for Innovation Medicine University of Verona, Italy; [7]Radiology Unit, Department of Pathology and Diagnostics, Azienda Ospedaliera Universitaria Integrata, Verona, Italy; [8]Neurology A, Azienda Ospedaliera Universitaria Integrata di Verona, Italy; [9]Institute of Life Sciences, Swansea University, United Kingdom; [10]Centre for Neuroscience, Department of Medicine, Charing Cross Hospital, Imperial College London, United Kingdom; and [11]Research Center for Clinical Neuroimmunology and Neuroscience Basel (RC2NB), University Hospital and University of Basel, Switzerland.

The Article Processing Charge was funded by University of Verona.

Glossary

AUC = area under the curve; **DIR** = double inversion recovery; **FLAIR** = fluid-attenuated inversion recovery; **FOV** = field of view; **GM** = gray matter; **HR** = hazard ratio; **MALF** = multiatlas-based likelihood fusion; **MS** = multiple sclerosis; **NEX** = number of excitations; **OOB** = out of bag; **PPI** = protein-protein interaction; **RF** = random forest; **ROC** = receiver operating characteristic; **TE** = echo time; **TFE** = turbo field echo; **TR** = repetition time; **WM** = white matter.

Introduction

Multiple sclerosis (MS) is an autoimmune demyelinating disease of the CNS, affecting primarily young adults and leading to significant neurologic disability.[1-3]

Initial observations from natural history large-cohort studies supported a two-staged disease model, in which most patients initially experience a relapsing-remitting course (RRMS) with prominent focal inflammatory activity, underlying acute neurologic relapses, subsequently followed by a progressive and irreversible disability accumulation (secondary progressive MS).[1-3] However, emerging evidence suggests a biological continuum in which mechanisms underlying relapses and progression coexist from early disease stages,[4-6] arguing against the two-stage dogmatic MS model. Even among young adults with RRMS and no ongoing inflammatory clinical attacks, a "smoldering" biological activity with steady and continuous progression of disability has been shown to be the major determinant of permanent confirmed disability accumulation over time.[2,7-10]

Such progression independent of relapse activity (PIRA) represents an unmet therapeutic and clinical need because the underlying processes are only poorly depicted by those MRI measures already adopted in clinical practice and their relation to other surrogate markers is a matter of ongoing debate.[4] Many definitions of PIRA have been proposed.[10,11] In particular, the occurrence of subclinical, MRI-detectable, inflammatory activity has been incorporated in some refined definitions, considering its potential interference with clinical findings. Thus, terms such as "true PIRA," "nonactive PIRA," and "progression independent of relapse and MRI activity, PIRMA") have been suggested, with the latter definition including absence of imaging signs of acute MRI activity close to the PIRA event date.[10]

An increasing body of evidence supports that intrathecal meningeal and perivascular inflammation, associated with gray matter (GM) damage and ongoing tissue damage,[11-14] plays a key role in determining the gradual disability accumulation from the earliest stages of the disease. Indeed, previous studies suggested that brain and cortical atrophy are pathologic substrates of PIRA, further highlighting the key contribution of the GM damage to disease progression.[7,15,16] In a previous study, by combining molecular neuropathology of progressive MS cases at postmortem analysis and both imaging and CSF analysis in patients with MS at the time of diagnosis, we demonstrated a common intrathecal (meningeal and CSF) inflammatory profile linked to increased cortical pathology.[17] This profile includes molecules associated with sustained B-cell activity and lymphoid neogenesis and is predictive of subsequent disease activity and cortical atrophy accumulation in early RRMS.[17,18]

In this study, we set out to determine a specific CSF profile and MRI measures of intrathecal compartmentalized inflammation that associate with and possibly predict PIRA and PIRMA in early RRMS.

Methods

Study Design

We analyzed clinical, CSF, and MRI data of 80 patients with RRMS, followed prospectively for 5 years from the time of diagnosis, at the MS Center of Verona, University Hospital, Verona, Italy. Inclusion criteria were as follows: (1) a diagnosis of RRMS according to McDonald revised 2017 diagnostic criteria[19]; (2) the availability of CSF obtained at the time of diagnosis; (3) a 3T brain MRI acquired within 1 week from the lumbar puncture.

The lumbar puncture was performed at the time of diagnosis and, after the diagnosis, all patients were treated with dimethyl fumarate or teriflunomide after study inclusion.

Medical history review and laboratory analysis excluded concurrent infections and systemic disorders.

Clinical Data

Participants underwent a neurologic evaluation using the Expanded Disability Status Scale (EDSS)[20] performed by 2 certified raters (M.C., D.M.) at the time of the diagnosis and every 6 months for 5 years, with additional visits in case of relapses.

Any acute disease activity with particular regard of relapses[21] or new ore enlarging MRI lesions was recorded.

Patients were included in the PIRA group when the following criteria were fulfilled: (1) a baseline/reference score, applied to set a new reference score every time the EDSS score was higher than the previous measure and confirmed at the following visit; (2) a clinically significant increase in the EDSS score of 1.5 points or more from an EDSS score of 0, 1.0 point or more from an EDSS score of 1.0–5.0, or 0.5 points or more from an EDSS score of 5.5 or more; (3) an increase in the

EDSS score not determined within 30 days before and 90 days after the onset of an investigator-reported relapse; (4) a confirmation EDSS score assigned at least 6 months after the initial disability increase.[10] The definition of PIRMA further required the exclusion of imaging signs of acute MRI activity (new or enlarging lesions or gadolinium-enhancing lesions) within 180 days before and after the PIRA event.[10,22]

CSF Analysis

We collected CSF samples at the time of the diagnosis, at least 1 month after a preceding relapse, and within 1 week from the MRI, according to the Consensus Guidelines for CSF and Blood Biobanking.[23] After centrifugation, we stored the supernatant at −80°C. We analyzed the CSF levels of 68 inflammatory mediators using a combination of immune-assay multiplex techniques based on the Luminex technology (40-Plex and 37-Plex, Bio-Plex X200 System equipped with a magnetic workstation; BioRad, Hercules, CA), as previously described.[18] All samples were duplicated in the same experiment and in 2 consecutive experiments to verify the reproducibility and consistency of results. The CSF concentration of each protein detected during the analysis was normalized to the total protein concentration of each CSF sample (measured by the Bradford assay).[18,19] Finally, CSF/serum albumin ratio and presence of CSF-restricted oligoclonal bands were recorded.

MRI Analysis

MRI Acquisition Protocol

Participants underwent a 3T Philips Achieva MRI acquisition at the Radiology Unit of the University Hospital of Verona at the time of diagnosis and every year, with additional evaluations in case of relapses. The following image sets were acquired:

1. 3D T1-weighted turbo field echo (TFE), with repetition time (TR) = 8.4 ms, echo time (TE) = 3.7 ms, voxel size = 1 × 1 × 1 mm^3, field of view (FOV) = 240 × 240 × 180, number of excitations (NEX) = 1, and acquisition time = 5:05 minutes
2. 3D fluid-attenuated inversion recovery (FLAIR) with TR/TE = 8,000/292 ms, inversion time (TI) = 2350 ms, voxel size = 1 × 1 × 1 mm^3, FOV = 240 × 240 × 180, NEX = 1, and acquisition time = 4:48 minutes
3. 3D double inversion recovery (DIR) with TR/TE = 5,500/292 ms, TI = 2,550 ms, delay 450 ms, voxel size = 1 × 1 × 1 mm^3, FOV = 240 × 240 × 180, NEX = 3, and acquisition time = 10:49 minutes
4. 3D T1-weighted TFE postcontrast sequence with the same parameters of the precontrast sequence. The gadolinium-based contrast agent adopted was gadobutrol, 0.1 mL/kg body weight (0.1 mmol/kg), with an average delay between injection and MRI acquisition of 10 minutes.

All images were quality-checked for scanner inhomogeneities and artifacts.

Image Processing

White matter (WM) lesions were automatically segmented on FLAIR images using the Lesion Segmentation Tool implemented in Statistical Parameter Mapping software on Matlab 2020b, and T2 hyperintense WM lesion masks, WM lesion volume (WMLv), and number (WMLn) were obtained. We used the T2 lesion masks to fill hypointensities on 3D T1-weighted images. New or enlarging T2 WM lesions were visually evaluated by a neuroradiologist with extensive experience in MS (FBP).

After lesion filling, we automatically segmented and parcellated the brain using multiatlas-based likelihood fusion (MALF) and FreeSurfer software to obtain mean global and regional cortical thickness (CTh) and GM volume. WM lesion filling was performed to reduce the risk of bias and improve the accuracy of CTh measure.[24]

Two observers (D.M., M.C.) with experience in evaluation of cortical lesions (CLs) manually segmented cortical lesions (and created a CL mask) and independently evaluated CL number on DIR images, following the recommendations for CL scoring in patients with MS.[25] In case of different evaluations, a decision was taken by consensus of both operators. Owing to the suboptimal performance of the MRI in visualizing subpial lesions, this analysis could have taken into account mainly the intracortical and leukocortical lesions. We used FSL to estimate the CL volume (CLv) using the CL masks.

Statistical Analysis

R (version 4.1) and GraphPad Prism (version 9) were used for statistical analysis.

Clinical Characteristics and Demographics

Mann-Whitney, χ^2, and Fisher exact tests were used when appropriate to assess differences between participants with and without PIRA. The analyses were repeated to assess differences between participants with and without PIRMA.

CSF and MRI Feature Selection and Prediction of PIRA

Random forest (RF) analysis was used to identify the baseline CSF molecules most associated with and best discriminating participants who experienced PIRA by the end of the follow-up.

RF analysis was also applied to baseline MRI measures, including GM regional thickness and volumes extracted from MALF, WMLn, WMLv, CLn, and CLv, and mean global CTh measures to identify the baseline MRI measures that best discriminate between participants with and without PIRA.

The cohorts were split into training (80%) and testing (20%) sets. The RF (1,000 trees, 8 variables tried at each split) was fitted on the training set, and the testing set was used to evaluate its performance. The abovementioned statistical analyses were repeated to discriminate participants with and without PIRMA.

Univariate estimates of the hazard ratios (HRs) of CSF cytokines and MRI markers identified with the RF analysis were calculated according to Cox regression analysis. Finally, variables significantly associated with the occurrence of PIRA ($p < 0.05$) were tested in a multivariate Cox proportional regression model, also including demographic factors (age and sex).

Pathway Analysis

To better investigate the CSF molecular profile associated with PIRA, we used STRING[26] analysis to quantify module connectivity and enriched biological functions. Module connectivity was evaluated by the protein-protein interaction (PPI) enrichment p value. A low PPI p value indicated that the nodes (proteins) were not random and that the observed number of edges (the interaction between proteins) was significant. Strength and false discovery rate measures were used to evaluate how significant the enrichment effect was for each biological process detected by the pathway analysis.

Receiver Operating Characteristic Analysis

The ability of CSF cytokines and MRI parameters evaluated at the time of diagnosis to discriminate between patients with and without PIRA was tested with the area under the receiver operating characteristic curves (AUC-ROCs). The predictive model included the variables that showed the best association with PIRA in the RF model and age. The Youden method was applied to determine the optimal threshold, specificity, and sensitivity. The discriminating ability of a multiparametric model incorporating both CSF cytokines and MRI variables was also tested.

Standard Protocol Approvals, Registrations, and Patient Consents

The study was approved by the Ethics Committee of the University of Verona (MSBio Biological Bank, protocol number 66418), and informed consent was collected from all participants.

Data Availability

Anonymized data not published within this article will be made available by request from any qualified investigator.

Results

Study Cohort

The demographic and clinical characteristics of the 80 patients with RRMS included in the study are presented in Table 1. During the follow-up, 49 patients experienced disease activity and 23 (28.8%) patients experienced a PIRA event (mean time to event 2.7 ± 1.1 years) with a mean EDSS increase of 1.5 ± 0.6. Of these, 8 developed new or enlarged, asymptomatic brain lesions (mean time to event 3.2 ± 1.5) and 5 experienced a relapse apart from the PIRA event (mean time to event 2.1 ± 2.0).

At diagnosis, in comparison with those without PIRA, participants with PIRA were older ($p = 0.017$) and had higher EDSS score ($p < 0.001$), higher WMLv ($p < 0.001$), higher WMLn ($p < 0.01$), higher CLn ($p = 0.032$), and higher CLv ($p = 0.039$). In addition, they were distinguished by baseline lower whole-brain GM volume ($p < 0.001$) and lower mean CTh ($p = 0.008$) when compared with the no PIRA group (Table 1). Clinical, demographic, and radiologic characteristics of patients without radiologic activity with or without PIRMA at baseline are provided in eTable 1.

CSF Analysis

CSF Markers of the PIRA Group

Compared with those without PIRA, at the time of diagnosis, patients with PIRA had different CSF values of many proinflammatory cytokines/chemokines (Table 2, Figure 1). The RF analysis revealed the CSF markers that best distinguished patients experiencing PIRA events (Figure 2A). The model had an out of bag (OOB) on the training set of 32.8% and achieved an accuracy of 0.69 when applied to the testing set.

Univariate Cox regression showed a significant association between higher levels of sTNFR1 (HR 8.37 [1.86–37.55], $p = 0.008$), sTNFR2 (HR 3.24 [1.07–9.79], $p = 0.040$), and LIGHT (HR 1.59 [1.00–2.55], $p = 0.044$) and risk of experiencing PIRA. At the multivariate Cox regression analysis, after adjusting for age and sex, sTNFR1 (HR 10.11 [2.61–39.10], $p = 0.001$), sTNFR2 (HR 5.05 [1.63–15.64], $p = 0.005$), and LIGHT (HR 1.79 [1.11–2.88], $p = 0.018$) were confirmed as independent predictors of PIRA (eTable 2).

All the selected molecules associated with PIRA were confirmed to be involved in chronic inflammatory processes, particularly the recruitment of adaptive and innate immune cells through cytokine and chemokine activity by STRING pathway analysis. The cellular signaling in response to TNF and TNF superfamily molecules and the negative regulation of extracellular matrix protein secretion were highlighted (eFigure 1 and eTable 3).

CSF Markers of PIRMA

Among patients who experienced PIRMA (marker values in eTable 4), the RF model highlighted those CSF molecules predictive of disability accumulation, which were not correlated with any clinical and radiologic focal inflammatory activity (Figure 2B). The model provided an OOB on the training set of 41.7% and achieved an accuracy of 0.56 on the testing set. Univariate Cox regression confirmed sTNFR1 (HR 6.27 [1.02–38.60], $p = 0.048$) and LIGHT (HR 1.81 [1.03–3.19], $p = 0.040$) as significantly increased among patients with PIRMA events. Multivariate analysis, adjusted for age and sex, confirmed sTNFR1 (HR 6.91 [1.28–37.27], $p = 0.025$) and LIGHT (HR 1.91 [1.09–3.34], $p = 0.025$) levels as independent intrathecal-based molecular predictors of PIRMA.

MRI Analysis

MRI Markers Associated With PIRA

Compared with those without PIRA, patients with PIRA events showed lower baseline GM thickness and volume in

Table 1 Demographic, Clinical, and MRI Characteristics at Diagnosis in the Whole Study Cohort and According to Occurrence of PIRA

	RRMS	PIRA	No PIRA	*p* Value
N (%)	80	23 (29)	57 (71)	
Age (y; mean [SD])	39.3 [12.3]	44.0 [10.7]	37.4 [12.4]	0.017
Sex (M/F)	16/64	5/18	11/46	0.768
Median EDSS score [25th–75th interquartile range]	2[1–3]	3[2–4]	1.5[1–2]	<0.001
OCBs (positive/negative)	60/20	17/6	43/14	0.99
CSF/serum albumin ratio [SD]	5.02 [1.61]	5.02 [1.66]	5.02 [1.61]	0.99
Whole-brain WM volume (mm^3; mean [SD])	696,300.02 [48,623.0]	675,945.35[56,075.5]	704,033.1 [43,574.6]	0.059
Whole-brain GM volume (mm^3; mean [SD])	787,767 [65,277.39]	748,688.21 [60,539.5]	802,183.4 [61,299.6]	<0.001
Mean cortical thickness (mm^3; mean [SD])	2.42 [0.09]	2.37 [0.11]	2.43 [0.08]	0.008
WMLn (mean [SD])	20.3 [15.8]	27.1 [13.1]	17.5 [16.2]	<0.01
WMLv (mm^3; mean [SD])	3.8 [5]	7.54 [5.77]	2.33 [3.79]	<0.001
Spinal cord lesions (mean [SD])	0.49 [0.95]	0.70 [1.18]	0.40 [0.84]	0.311
Gd+ lesions (mean [SD])	0.16 [0.54]	0.08 [0.29]	0.19 [0.61]	0.751
CLn (mean [SD])	4.72 [7.67]	6.13 [6.07]	2.91 [3.59]	0.032
CLv (mm^3; mean [SD])	219.8 [399.73]	571.87 [619.36]	260.32 [340.10]	0.039

Abbreviations: CLn = cortical lesion number; CLv = cortical lesion volume; EDSS = Expanded Disability Status Scale; F = female; Gd+ lesions = gadolinium-enhancing lesions; GM = gray matter; M = male; OCBs = oligoclonal bands; PIRA = progression independent of relapse activity; RRMS = relapsing-remitting multiple sclerosis; WM = white matter; WMLn = white matter lesion number; WMLv = white matter lesion volume.
Statistical comparisons of baseline characteristics of participants with or without PIRA are shown.

many brain areas (Table 3). The RF model was applied to all variables and had an OOB on the training set of 28.3%, achieving a prediction accuracy of 0.75 on the testing set. The most important features in identifying patients with PIRA were the baseline CLn and volume/thickness of several cortical and deep GM regions (Figure 3A).

Univariate Cox regression analysis of these MRI parameters showed that caudate (HR 0.99 [0.99–1], $p = 0.025$), putamen (HR 0.99 [0.99–1], $p = 0.041$), and thalamus (HR 0.99 [0.98–0.99], $p = 0.001$) volumes, alongside CTh of the middle frontal gyrus (HR 0.03 [0.03–0.38], $p = 0.006$) and CLn (HR 1.13 [1.03–1.23], $p = 0.013$), were associated with higher risk of experiencing PIRA. In the Cox multivariate analysis, after adjusting for age and sex, thalamic volume (HR 0.98 [0.97–0.99], $p = 0.005$), CTh of the middle frontal gyrus (HR 0.05 [0.01–0.72], $p = 0.028$), and CLn (HR 1.15 [1.05–1.25], $p = 0.003$) were confirmed as independent predictors of PIRA (eTable 5).

MRI Markers Associated With PIRMA

The abovementioned analysis of the MRI measures was repeated in the PIRMA subgroup (eTable 6). The RF provided an OOB on the training set of 28.1% and achieved a prediction accuracy of 0.5 on the testing set. The model showed that the most important baseline features in identifying participants with PIRMA events were the volume of thalamus and pallidum; the CTh of supramarginal gyrus, planum polare, planum temporale, and posterior cingulate gyrus; and CLn (Figure 3B). Univariate Cox regression analysis on the statistically significant features identified by the RF showed that CLn (HR 1.17 [1.06–1.29], $p = 0.003$) significantly increased in patients with PIRMA. Multivariate analysis, after adjusting for age and sex, confirmed this result (HR 1.17 [1.05–1.30], $p = 0.004$).

ROC Analysis

The results of the ROC analysis for each CSF cytokine selected by the RF method are displayed in eFigure 2 and detailed in eTable 7. Similarly, eFigure 3 and eTable 8 present the results for MRI parameters. The combined model incorporating CSF markers provided an AUC of 0.82 [0.70–0.94] while the AUC for combined MRI parameters was 0.80 [0.68–0.92]. The model incorporating both CSF markers and MRI parameters achieved an AUC of 0.87 [0.78–0.96] (Figure 4).

Discussion

The identification of candidate markers of early PIRA, as well as defining its pathologic determinants,[4] represents an unmet need, hindering the implementation of a personalized therapeutic approach starting at the time of diagnosis.[8]

Table 2 Cytokines and Chemokines Values in the Whole Cohort and According to Occurrence or Not of PIRA

	Total MS (n = 80)	No PIRA (n = 57)	PIRA (n = 23)	*p* Value
CCL21	1,701.61 ± 1,074.09	1,746.92 ± 1,092.68	1,589.32 ± 1,041.70	0.428
CXCL13	13.90 ± 29.50	9.20 ± 15.01	25.30 ± 48.31	0.144
CXCL5	748.88 ± 610.68	778.57 ± 616.55	680.45 ± 604.85	0.445
CCL11	82.01 ± 85.53	83.01 ± 78.48	79.60 ± 102.57	0.536
CCL24	47.77 ± 44.37	43.69 ± 42.28	54.42 ± 49.35	0.186
CCL26	44.63 ± 54.73	41.15 ± 49.14	52.96 ± 66.74	0.425
CX3CL1	335.28 ± 238.89	320.78 ± 224.21	371.21 ± 273.99	0.750
GMCSF	97.69 ± 98.78	91.36 ± 82.67	112.55 ± 130.05	0.711
CXCL1	102.96 ± 97.52	95.84 ± 91.25	120.63 ± 111.79	0.398
CXCL2	62.35 ± 73.54	61.19 ± 77.55	65.60 ± 62.77	0.560
CCL1	49.83 ± 42.10	43.57 ± 36.38	63.29 ± 50.78	0.091
CXCL10	434.44 ± 539.45	419.97 ± 580.48	470.29 ± 430.54	0.253
CXCL11	78.59 ± 546.82	101.08 ± 647.61	22.84 ± 39.97	0.998
CCL2	499.84 ± 644.05	448.05 ± 653.11	628.19 ± 616.07	0.071
CCL8	222.36 ± 637.78	206.80 ± 685.10	260.95 ± 513.56	0.153
CCL7	53.86 ± 46.59	50.88 ± 42.77	61.53 ± 55.67	0.589
CCL13	31.64 ± 61.02	40.10 ± 68.80	9.49 ± 21.68	0.490
CCL22	44.88 ± 82.17	47.47 ± 93.36	38.95 ± 48.63	0.349
MIF	1,616.21 ± 1,648.13	1,441.24 ± 1,515.04	2,049.81 ± 1906.72	0.165
CXCL9	72.44 ± 69.32	76.22 ± 75.02	63.09 ± 52.96	0.704
CCL3	5.85 ± 5.03	5.14 ± 3.29	7.61 ± 7.68	0.420
CCL15	439.30 ± 397.49	402.37 ± 305.24	530.83 ± 563.85	0.642
CCL20	1.66 ± 1.76	1.38 ± 1.68	2.43 ± 1.81	0.052
CCL19	117.95 ± 103.67	118.08 ± 112.09	117.64 ± 82.33	0.471
CCL23	12.90 ± 17.61	12.83 ± 19.64	13.09 ± 11.29	0.506
CXCL16	1,799.83 ± 1,379.65	1,730.89 ± 1,282.93	1,970.66 ± 1,613.28	0.792
CXCL12	2,162.25 ± 1965.89	1,954.20 ± 1864.28	2,677.86 ± 2,154.28	0.102
CCL25	120.56 ± 74.16	119.43 ± 67.45	123.36 ± 90.31	0.874
TNF	36.02 ± 34.37	34.38 ± 35.53	40.10 ± 31.70	0.277
sTNFR1	4,362.94 ± 3,238.43	3,726.40 ± 2024.07	5,940.43 ± 4,855.88	0.010
sTNFR2	1,032.57 ± 1,089.65	877.62 ± 938.05	1,416.57 ± 1,344.31	0.087
TWEAK	2,134.63 ± 2,242.36	2,009.22 ± 2,133.18	2,445.41 ± 2,516.15	0.472
APRIL	49,874.46 ± 57,941.67	52,461.98 ± 63,825.21	43,461.91 ± 37,938.89	0.823
BAFF	10,596.84 ± 7,175.78	10,287.36 ± 6,315.24	11,363.79 ± 9,084.11	0.874
LIGHT	261.56 ± 428.75	178.97 ± 290.36	455.45 ± 613.10	0.013
sCD30	1,658.38 ± 1,482.91	1,663.60 ± 1,466.19	1,645.68 ± 1,556.26	0.868
IFNg	16.08 ± 21.42	13.63 ± 17.38	21.96 ± 28.52	0.092
IFNalfa2	17.13 ± 18.91	15.60 ± 16.65	20.63 ± 23.38	0.301
IFNbeta	34.44 ± 29.60	31.56 ± 26.42	41.65 ± 36.04	0.366

Continued

Table 2 Cytokines and Chemokines Values in the Whole Cohort and According to Occurrence or Not of PIRA *(continued)*

	Total MS (n = 80)	No PIRA (n = 57)	PIRA (n = 23)	*p* Value
IL28a	188.38 ± 492.68	200.89 ± 554.11	159.19 ± 315.08	0.211
IL29	40.54 ± 39.65	39.81 ± 39.84	42.19 ± 40.16	0.580
sIL6R-beta	88,235.33 ± 70,647.29	85,402.97 ± 62,638.38	95,257.14 ± 88,672.21	0.866
IL1beta	2.74 ± 3.55	2.55 ± 3.08	3.24 ± 4.57	0.860
IL4	20.57 ± 17.25	17.98 ± 14.53	26.68 ± 21.58	0.148
IL6	25.97 ± 49.78	27.52 ± 55.08	22.12 ± 33.97	0.411
IL8	68.22 ± 83.10	63.17 ± 80.81	80.75 ± 89.12	0.519
IL10	21.41 ± 19.06	21.49 ± 18.53	21.22 ± 20.76	0.784
IL16	108.09 ± 126.80	95.46 ± 107.80	139.40 ± 163.45	0.295
sIL6Ra	3,926.30 ± 2,872.81	3,765.42 ± 2,648.99	4,325.01 ± 3,397.16	0.858
IL11	3.96 ± 13.23	5.06 ± 15.49	1.15 ± 1.28	0.920
IL12 (p40)	18.29 ± 19.87	15.88 ± 17.51	24.57 ± 24.47	0.153
IL12 (p70)	15.80 ± 25.94	21.17 ± 30.08	5.06 ± 7.05	0.007
IL19	69.63 ± 52.26	60.62 ± 41.26	89.79 ± 67.95	0.115
IL20	44.83 ± 68.18	40.57 ± 61.29	54.45 ± 82.39	0.132
IL22	34.68 ± 32.81	29.77 ± 26.32	46.42 ± 43.15	0.056
IL26	925.98 ± 949.61	1,027.41 ± 1,060.73	692.27 ± 576.95	0.351
IL27	192.21 ± 167.77	160.55 ± 145.70	276.61 ± 196.35	0.009
IL32	153.69 ± 179.89	159.61 ± 189.25	139.53 ± 158.30	0.579
IL34	561.51 ± 576.99	616.96 ± 650.27	440.53 ± 353.76	0.486
IL35	270.48 ± 194.98	263.95 ± 189.31	286.68 ± 211.92	0.658
MMP1	860.29 ± 1,029.41	767.02 ± 991.57	1,116.80 ± 1,112.79	0.091
MMP2	1,638.62 ± 4,814.30	2,074.25 ± 5,668.65	577.93 ± 425.77	0.808
Osteocalcin	654.25 ± 408.04	640.80 ± 418.28	687.58 ± 388.45	0.744
Osteopontin	73,914.62 ± 77,298.09	63,978.32 ± 71,800.86	98,539.37 ± 86,273.8425	0.049
Pentraxin	282.49 ± 332.48	295.87 ± 362.17	249.90 ± 249.92	0.783
TSLP	40.10 ± 49.51	39.60 ± 55.09	41.33 ± 32.79	0.114
sCD163	47,917.11 ± 33,673.06	47,618.24 ± 37,419.12	48,657.80 ± 22,510.35	0.408
Chitinase3like1	44,664.38 ± 35,907.8096	41,233.66 ± 33,506.79	53,166.59 ± 40,818.52	0.155

Abbreviations: APRIL = a proliferation-inducing ligand; BAFF = B-cell activating factor; C-C motif chemokine 22; CCL1 = chemokine (C-C motif) ligand 1; CCL13 = chemokine (C-C motif) ligand 13; CCL15 = chemokine (C-C motif) ligand 15; CCL19 = chemokine (C-C motif) ligand 19; CCL2 = chemokine (C-C motif) ligand 2; CCL20 = chemokine (C-C motif) ligand 20; CCL21 = chemokine (C-C motif) ligand 21; CCL22; CCL23 = chemokine (C-C motif) ligand 23; CCL24 = chemokine (C-C motif) ligand 24; CCL25 = chemokine (C-C motif) ligand 25; CCL26 = chemokine (C-C motif) ligand 26; CCL3 = chemokine (C-C motif) ligand 3; CCL7 = chemokine (C-C motif) ligand 7; CCL8 = chemokine (C-C motif) ligand 8; CX3CL1 = chemokine (C-X3-C motif) ligand 1; CXCL1 = chemokine (C-X-C motif) ligand 1; CXCL10 = chemokine (C-X-C motif) ligand 10; CXCL11 = chemokine (C-X-C motif) ligand 11; CXCL12 = chemokine (C-X-C motif) ligand 12; CXCL13 = chemokine (C-X-C motif) ligand 13; CXCL5 = chemokine (C-X-C motif) ligand 5; CCL11 = chemokine (C-C motif) ligand 11; CXCL16 = chemokine (C-X-C motif) ligand 16; CXCL2 = chemokine (C-X-C motif) ligand 2; CXCL9 = chemokine (C-X-C motif) ligand 9; GM-CSF = granulocyte-macrophage colony-stimulating factor; IFNalfa2 = interferon alpha-2; IFNbeta = interferon beta; IFNgamma = interferon gamma; IL10 = interleukin-10; IL11 = interleukin-11; IL12(p40) = interleukin-12 or cytotoxic lymphocyte maturation factor p40; IL12(p70) = interleukin-12 or cytotoxic lymphocyte maturation factor p70; IL16 = interleukin-16; IL19 = interleukin-19; IL1beta = interleukin-1 beta; IL20 = interleukin-20; IL22 = interleukin-22; IL26 = interleukin-26; IL27 = interleukin-27; IL28A = interleukin-28 A; IL29 = interleukin-29; IL32 = interleukin-32; IL34 = interleukin-34; IL35 = interleukin-35; IL4 = interleukin-4; IL6 = interleukin-6; IL8 = interleukin-8; LIGHT = tumor necrosis factor superfamily member 14; MIF = macrophage migration inhibitor factor; MMP1 = matrix metallopeptidase 1; MMP2 = matrix metallopeptidase 2; osteocalcin = bone gamma-carboxyglutamic acid-containing protein; PIRA = progression independent of relapse activity; sCD163 = soluble-CD163 (cluster of differentiation 163); sCD30 = soluble tumor necrosis factor receptor superfamily 8; sIL6Ra = soluble interleukin-6 receptor alpha; sIL6Rbeta = soluble interleukin-6 receptor beta; sTNFR1 = soluble-tumor necrosis factor-receptor 1; sTNFR2 = soluble-tumor necrosis factor-receptor 2; TNF = tumor necrosis factor; TSLP = thymic stromal lymphopoietin; TWEAK = TNF-related weak inducer of apoptosis.
Values are expressed as pg/mL; means ± SD are reported.
The Mann-Whitney *U* test was adopted to compare the mean values of CSF molecules between participants with and without PIRA. Significant comparisons ($p < 0.05$) are reported in bold.

Figure 1 CSF Markers and PIRA

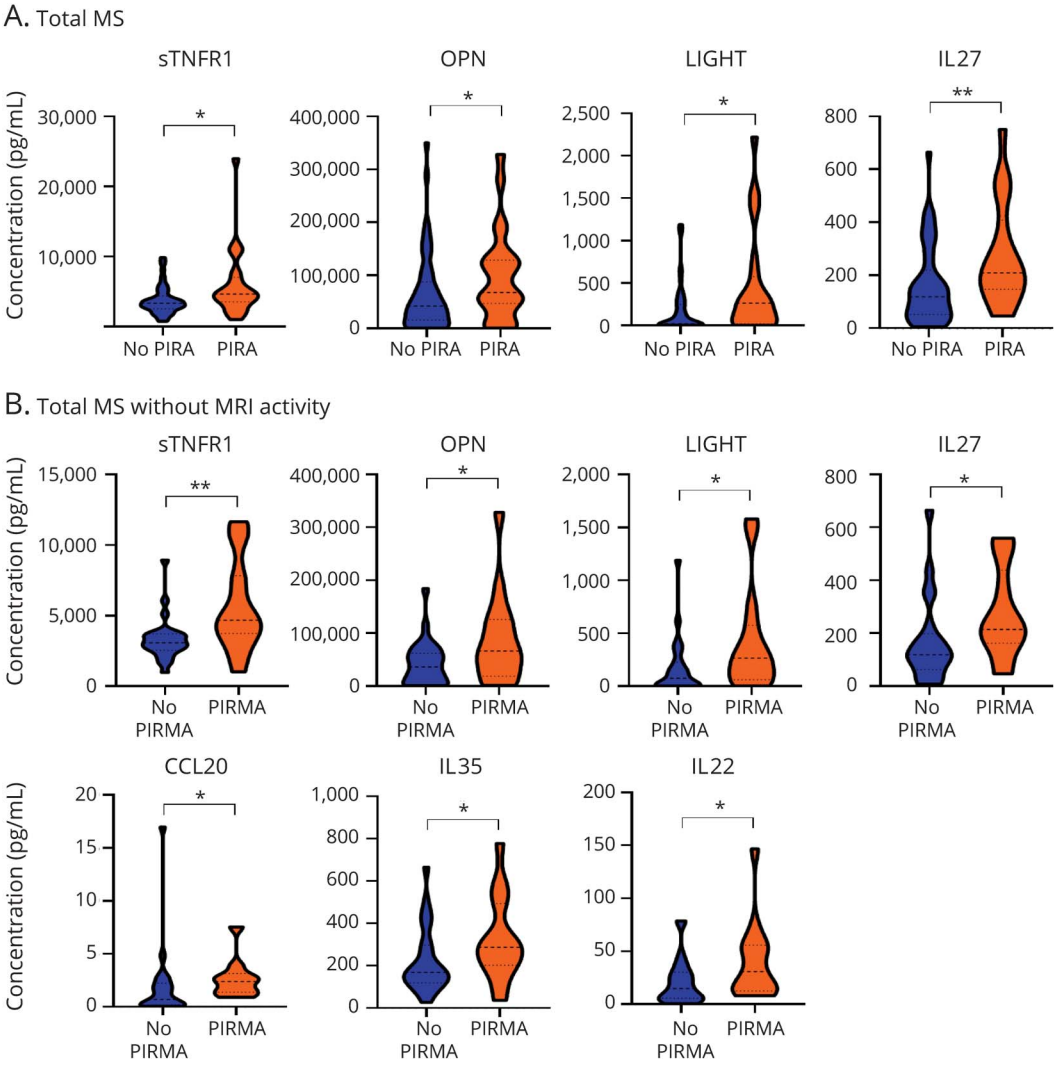

(A) CSF markers increased in patients with PIRA events. (B) Markers differentially increased in the subgroup of patients with PIRMA. CCL20 = chemokine (C-C motif) ligand 20; IL22 = interleukin-22; IL27 = interleukin-27; IL35 = interleukin-35; LIGHT = tumor necrosis factor superfamily member 14; OPN = osteopontin; PIRA = progression independent of relapse activity; PIRMA = progression independent of relapse and MRI activity; sTNFR1 = soluble-tumor necrosis factor-receptor 1. *$p < 0.05$, **$p < 0.01$

In this study, we compared the demographic, clinical, CSF, and MRI profile at diagnosis between patients with RRMS who experienced PIRA (or PIRMA) in the 5 years after the diagnosis and those who remained free of disability progression. Our analysis revealed that the risk of experiencing disability progression was associated with the altered expression of molecules related to the TNF superfamily and with specific MRI features including cortical lesion number, CTh of the frontal cortex, and volume of deep gray matter structures such as thalamus.

To identify whether molecular markers present at diagnosis can predict later development of PIRA, we assayed a range of inflammatory mediators that are potentially associated with MS pathobiology and progression. The analysis of the diagnostic CSF suggested that mechanisms underlying perivascular and meningeal inflammation are implicated in the development of early PIRA.

In particular, a specific CSF profile that included molecules of the TNF superfamily was found to be the best surrogate marker of PIRA, with LIGHT (also called TNFSF14) and sTNFR1 emerging as the most important predictors of occurrence of disability accumulation not related to acute attacks. LIGHT is a protein that coexists in both a membrane-bound and a soluble form. Although its functional role in CNS inflammatory response is only partially understood, the membrane-bound form may exert proinflammatory activity, including enhanced survival of $CD4^+$ memory T cells[27] and the costimulation of T cells,[28] while, after shedding, it decreases stimulatory signals and acts as a T-cell inhibitor by stabilizing the *cis* HVEM:BTLA complex.[29] Accordingly,

Figure 2 CSF Markers Associated With PIRA

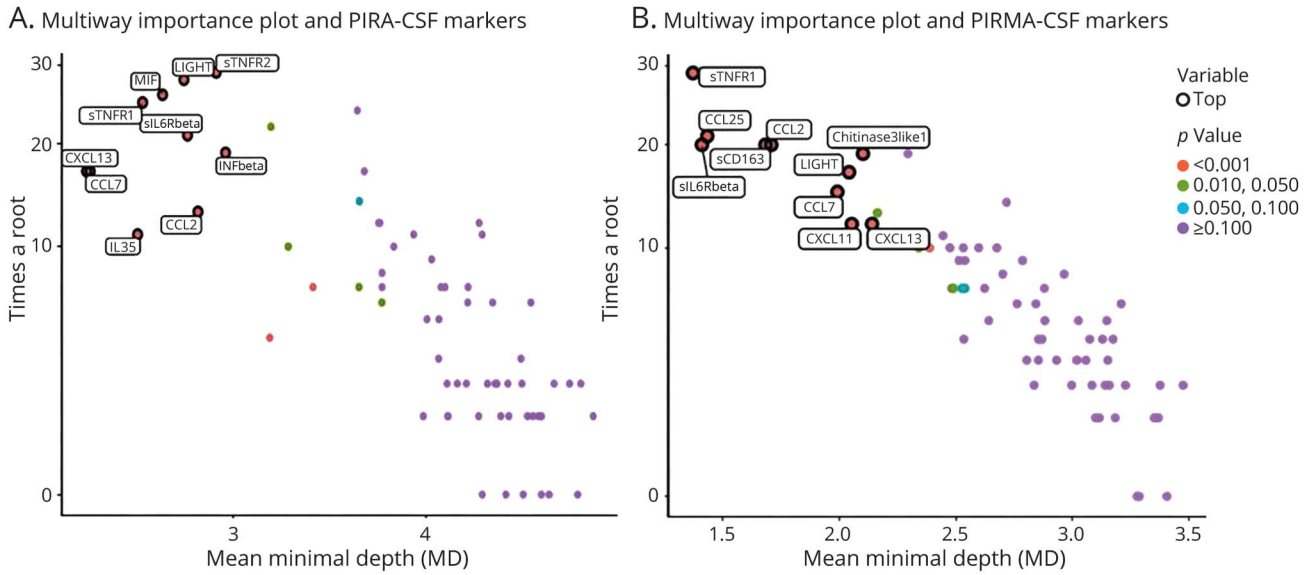

(A) Multiway importance plot: most important variables associated with PIRA. Minimal depth and times a root measures are shown. Lower minimal depth values indicate higher predictive accuracy while higher times a root measure indicates a higher predictive power. (B) Multiway importance plot: most important variables associated with PIRMA. CCL2 = chemokine (C-C motif) ligand 2; CCL25 = chemokine (C-C motif) ligand 25; CCL7 = chemokine (C-C motif) ligand 7; CXCL11 = chemokine (C-X-C motif) ligand 11; CXCL13 = chemokine (C-X-C motif) ligand 13; IL35 = interleukin-35; INFbeta = interferon beta; LIGHT = tumor necrosis factor superfamily member 14; MIF = macrophage migration inhibitor factor; PIRA = progression independent of relapse activity; PIRMA = progression independent of relapse and MRI activity; sCD163 = soluble-CD163 (cluster of differentiation 163); sIL6Rbeta = soluble interleukin-6 receptor beta; sTNFR1 = soluble-tumor necrosis factor-receptor 1; sTNFR2 = soluble-tumor necrosis factor-receptor 2.

a LIGHT gene variation was shown to increase the MS risk in a genome-wide association study[30] with increased serum levels among patients with disease activity and decreased levels among those treated with natalizumab.[31] Soluble LIGHT, through the interaction with the lymphotoxin-beta receptor (LTbetaR), seems to exert a proinflammatory role in an experimental hepatitis model[32] and has also been reported to contribute to the maintenance of lymphoid microenvironment including B-cell follicles in secondary lymphoid organs.[33] The results are in line with our previous studies,[17,18] where CSF LIGHT was found to be strongly related to the severity of cortical thinning over time.[18] Furthermore, molecules related to lymphoid recruitment, such as CXCL13, which we similarly found associated with cortical atrophy accumulation, were confirmed as candidate biomarkers of PIRA, further supporting the role of intrathecal inflammation, possibly related to the presence of meningeal tertiary lymphoid-like structures, as one of the principal determinants of disability progression that is manifest in the first years of the disease.

The STRING pathway analysis confirmed an inflammatory profile characterized by high and dysregulated levels of the TNF superfamily. Data on the role of TNF in the pathogenesis of MS and associated neuronal loss are convincing and consistent.[34] Patients with progressive MS are characterized by higher TNF levels that correlate with the degree of disability progression.[35] Accordingly, increased TNF detected in meninges and CSF highly correlated with GM demyelination at both the time of diagnosis and death,[18] with unbalanced levels of their receptor soluble molecules (sTNFR1 and sTNFR2), a finding also confirmed in patients at the time of diagnosis.[36] Gene expression profiling of both cortical lesions and normal-appearing GM confirmed that increased meningeal inflammation is associated with a shift in the balance of TNF signaling away from TNFR1/TNFR2, the first preferentially expressed on neurons and oligodendrocytes and the latter more expressed by astrocytes and microglia.[37,38] Finally, the persistent meningeal production in the animal model of TNF and IFNγ led to both subpial demyelination and neuronal loss, corroborating all these proteomic, transcriptomic, and pathologic evidence.[39]

In contrast with the increasing amount of evidence on the role of a dysfunctional TNF pathway in mediating MS progression, so far, therapies targeting TNF failed in halting disease activity. One possible explanation is the nonselectivity of the treatment, with absence of stimulation of TNFR2 that potentially leads to immune regulation and tissue protection. Efforts are then needed to develop new therapeutical anti-TNF strategies that could target the detrimental aspects of TNF pathway and be beneficial since early disease stages.

From the imaging point of view, the baseline number and volume of CLs were higher in those patients who developed PIRA events. This is not unexpected because several previous studies suggested a strong association between CLs and disease progression.[16] Moreover, in a 30-year longitudinal study, the number of CLs was the best marker of EDSS accumulation.[40]

Table 3 MRI Values of Regional Thickness/Volume at Diagnosis in the Whole Study Cohort and According to the Occurrence of PIRA

		End of follow-up		
	RRMS at diagnosis	PIRA	No PIRA	*p* Value
***N* (%)**	80	23 (29)	57 (71)	
Cerebellum (mm^3; mean [SD])	3.21 ± 0.48	2.97 ± 0.51	3.29 ± 0.45	0.014
Hippocampus (mm^3; mean [SD])	2.76 ± 0.26	2.77 ± 0.29	2.76 ± 0.24	0.911
Anterior cingulate gyrus (mm^3; mean [SD])	3.51 ± 0.35	3.34 ± 0.33	3.57 ± 0.54	0.019
Anterior insula (mm^3; mean [SD])	3.82 ± 0.37	3.69 ± 0.42	3.88 ± 0.34	0.052
Frontal pole (mm^3; mean [SD])	2.62 ± 0.24	2.56 ± 0.25	2.65 ± 0.24	0.177
Inferior temporal gyrus (mm^3; mean [SD])	3.67 ± 0.33	3.51 ± 0.25	3.73 ± 0.24	0.006
Middle cingulate gyrus (mm^3; mean [SD])	2.56 ± 0.29	2.42 ± 0.29	2.60 ± 0.28	0.018
Medial frontal cortex (mm^3; mean [SD])	3.15 ± 0.38	3.03 ± 0.40	3.19 ± 0.36	0.124
Middle frontal gyrus (mm^3; mean [SD])	2.34 ± 0.21	2.24 ± 0.24	2.38 ± 0.19	0.001
Medial postcentral gyrus (mm^3; mean [SD])	1.32 ± 0.29	1.21 ± 0.33	1.35 ± 0.27	0.037
Medial precentral gyrus (mm^3; mean [SD])	1.80 ± 0.35	1.67 ± 0.39	1.87 ± 0.31	0.053
Medial superior frontal gyrus (mm^3; mean [SD])	2.80 ± 0.34	2.68 ± 0.35	2.84 ± 0.33	0.065
Middle temporal gyrus (mm^3; mean [SD])	3.04 ± 0.29	2.87 ± 0.29	3.10 ± 0.27	0.003
Posterior cingulate gyrus (mm^3; mean [SD])	2.86 ± 0.32	2.70 ± 0.37	2.91 ± 0.29	0.035
Precuneus (mm^3; mean [SD])	2.28 ± 0.33	2.28 ± 0.33	2.47 ± 0.31	0.022
Parahippocampal gyrus (mm^3; mean [SD])	3.00 ± 0.35	2.88 ± 0.36	3.04 ± 0.33	0.139
Posterior insula (mm^3; mean [SD])	3.27 ± 0.39	3.12 ± 0.39	3.33 ± 0.38	0.037
Postcentral gyrus (mm^3; mean [SD])	1.51 ± 0.22	1.43 ± 0.22	1.54 ± 0.21	0.062
Planum polare (mm^3; mean [SD])	1.76 ± 0.29	1.64 ± 0.25	1.80 ± 0.29	0.013
Precentral gyrus (mm^3; mean [SD])	2.04 ± 0.28	1.94 ± 0.31	2.07 ± 0.27	0.041
Planum temporale (mm^3; mean [SD])	1.86 ± 0.29	1.73 ± 0.32	1.90 ± 0.36	0.030
Superior frontal gyrus (mm^3; mean [SD])	2.29 ± 0.20	2.20 ± 0.19	2.32 ± 0.20	0.011
Supplementary motor cortex (mm^3; mean [SD])	2.46 ± 0.34	2.28 ± 0.19	2.52 ± 0.20	0.008
Supramarginal gyrus (mm^3; mean [SD])	2.23 ± 0.21	2.15 ± 0.19	2.26 ± 0.20	0.013
Superior parietal lobule (mm^3; mean [SD])	1.72 ± 0.19	1.67 ± 0.18	1.73 ± 0.19	0.205
Superior temporal gyrus (mm^3; mean [SD])	2.38 ± 0.26	2.26 ± 0.18	2.42 ± 0.19	0.028
Temporal pole (mm^3; mean [SD])	3.75 ± 0.44	3.51 ± 0.44	3.84 ± 0.41	0.006
Inferior frontal gyrus (mm^3; mean [SD])	2.17 ± 0.23	2.05 ± 0.24	2.21 ± 0.21	0.005
Caudate (mm^3; mean [SD])	3,099.58 ± 480.44	2,897.98 ± 618.27	3,171.58 ± 403.29	0.010
Pallidum (mm^3; mean [SD])	1,425.96 ± 158.21	1,425.96 ± 158.21	1,348.90 ± 239.11	0.113
Putamen (mm^3; mean [SD])	4,239.86 ± 547.74	4,010 ± 534.47	4,321 ± 533.38	0.016
Thalamus (mm^3; mean [SD])	7,111 ± 547.74	6,503 ± 1,210.97	7,329.24 ± 855.95	0.002

Abbreviations: PIRA = progression independent of relapse activity; RRMS = relapsing-remitting multiple sclerosis.

Similarly, baseline deep GM atrophy emerged as a significant predictive factor in participants with PIRA. Basal ganglia atrophy and particularly thalamic atrophy have been repeatedly suggested as a key finding in MS pathology, associated with cognition, fatigue, and disability progression.[41-44]

Figure 3 MRI Markers Associated With PIRA

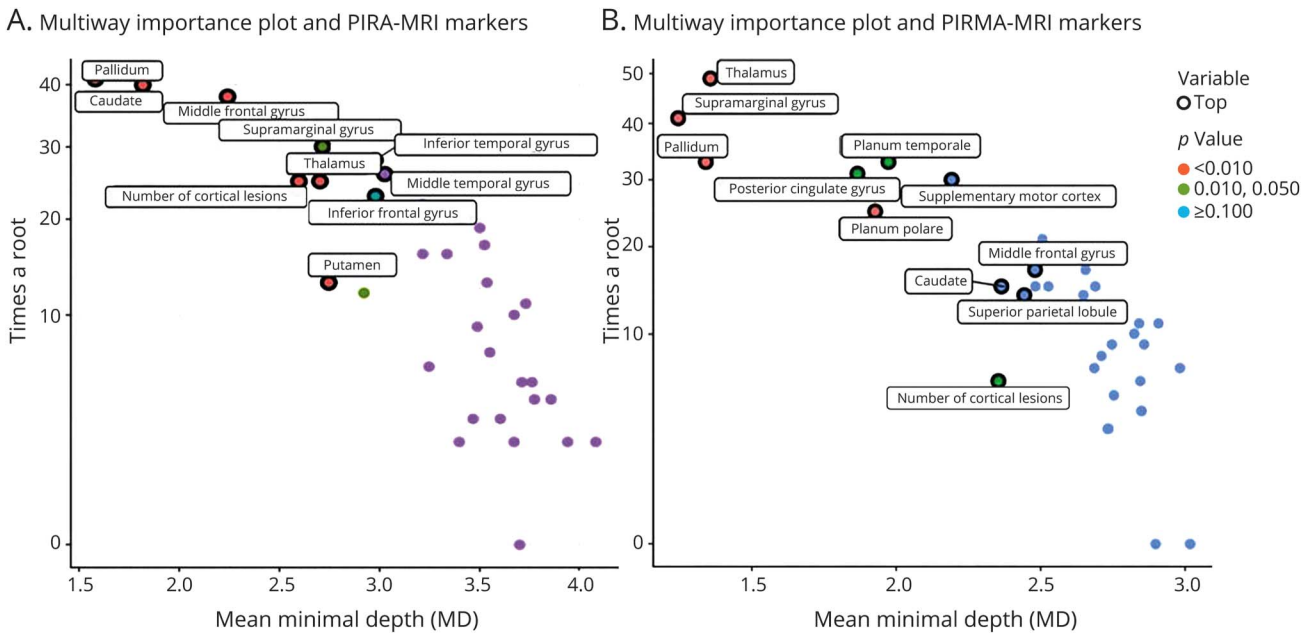

Multiway importance plot with the most important MRI variables associated with PIRA (A) and in a subgroup of patients with PIRMA (B). Minimal depth and times a root measures are shown. Lower minimal depth values indicate higher predictive accuracy while higher times a root measure indicates a higher predictive power. PIRA = progression independent of relapse activity; PIRMA = progression independent of relapse and MRI activity.

Such cortical and deep GM involvement could represent a surrogate marker of chronic compartmentalized inflammation and of the widespread MS neurodegeneration processes. Certainly, compartmentalized CNS inflammation, linked to the persistence of adaptive immune infiltrates in niches such as perivascular and meningeal spaces, in combination with glial cell activation and the presence of chronic expanding lesions, represents a key driver of disability accrual.[14,17] Particularly, subpial cortical demyelination, which represents the largest and most frequently observed lesion type of MS, is associated with B-cell and T-cell infiltrates in the adjacent meningeal sulci,[12] a key hallmark of

Figure 4 ROC Analysis

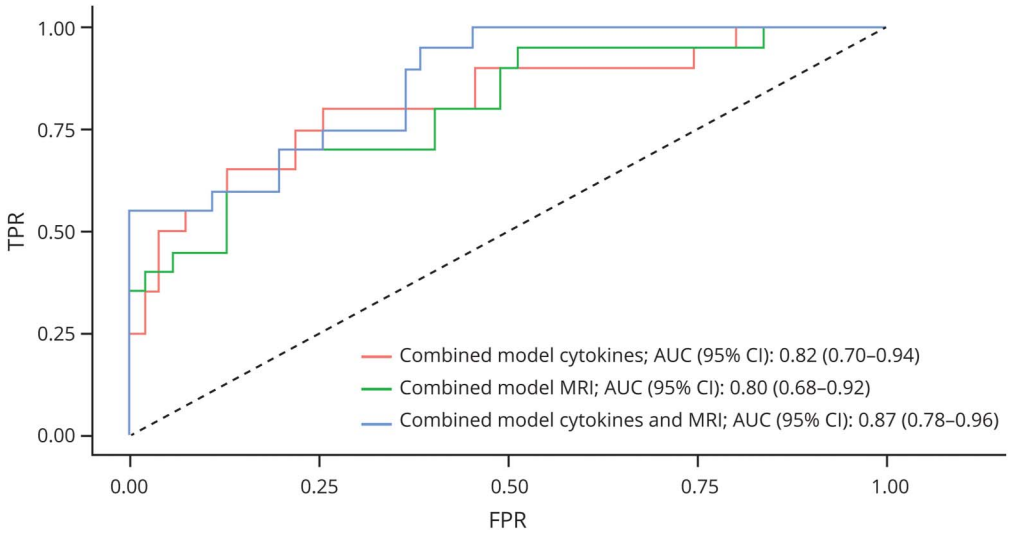

ROC analysis curves showing combined models with CSF and MRI markers. AUC = area under the curve; CI = confidence interval; CM = combined model; FBR = false-positive rate; ROC = receiver operating characteristic; TPR = true-positive rate.

compartmentalized inflammation. Gradients of tissue damage in the subpial tissue, a site adjacent to the CSF-filled space, are also seen at other structures such as the cerebellum and deep GM, including the thalamus.[45,46] These findings are in line with the hypothesis that inflammatory factors diffuse into the underlying tissues, either by influencing the activation status of CNS parenchymal cells to mediate tissue injury or by directly promoting a cytotoxic effect in the adjacent GM.[47] To evaluate the possible role of subclinical MRI activity, we performed an additional analysis on a group of patients with PIRMA. Notably, results from the CSF and MRI marker analysis of participants with PIRA were confirmed in patients with PIRMA, suggesting a common physiopathologic trait that underlies the risk of attaining PIRA regardless of acute inflammatory activity that is discernible on MRI.[48]

The work has a number of limitations. Beyond the early accumulation of focal and diffuse GM demyelination,[11,13] many other pathologic processes that have not been evaluated in our study may concur with PIRA, including the presence of demyelinating activity in chronic lesions,[48,49] spinal cord lesions, and atrophy[48] and possible altered remyelination mechanisms, all leading to premature and irreversible neuroaxonal damage. However, despite this, we still noticed a significant impact of our measured markers on PIRA.

The relatively low number of patients with PIRA and the absence of a validation cohort may limit the generalizability of our conclusions. Notably, we noticed a high proportion of patients with PIRA,[50] particularly if considering an early MS cohort. This finding could be explained by the relatively high age at which patients underwent the diagnostic lumbar puncture. Furthermore, the selection of a cohort of patients treated with 2 not high-efficacy treatments, potentially led to a homogeneous sample of participants but with a relatively higher risk of experiencing PIRA.[51]

Finally, a composite measure that includes upper limb function, walking speed, and cognitive testing would provide additional value to the clinical definition of PIRA.[10]

With the abovementioned limitations, we can suggest that (1) a specific intrathecal inflammatory and MRI profile present at diagnosis characterizes the subsequent risk of early PIRA and (2) anti-inflammatory therapies capable of modulating intrathecal inflammation may be effective in preventing PIRA events and should be subjected to further careful investigations.

Acknowledgment

The authors thank the patients with MS and the Laboratory of Neuropathology at LURM (University Laboratory of Medical Research), University of Verona.

Author Contributions

D. Marastoni: drafting/revision of the manuscript for content, including medical writing for content; major role in the acquisition of data; study concept or design; analysis or interpretation of data. E. Colato: drafting/revision of the manuscript for content, including medical writing for content; study concept or design; analysis or interpretation of data. M. Foschi: drafting/revision of the manuscript for content, including medical writing for content; study concept or design; analysis or interpretation of data. A. Tamanti: drafting/revision of the manuscript for content, including medical writing for content; major role in the acquisition of data; analysis or interpretation of data. S. Ziccardi: drafting/revision of the manuscript for content, including medical writing for content; major role in the acquisition of data; analysis or interpretation of data. C. Eccher: drafting/revision of the manuscript for content, including medical writing for content; major role in the acquisition of data. F. Crescenzo: drafting/revision of the manuscript for content, including medical writing for content; major role in the acquisition of data. A. Bajrami: drafting/revision of the manuscript for content, including medical writing for content; major role in the acquisition of data. G.M. Schiavi: drafting/revision of the manuscript for content, including medical writing for content; major role in the acquisition of data. V. Camera: drafting/revision of the manuscript for content, including medical writing for content; major role in the acquisition of data. D. Anni: drafting/revision of the manuscript for content, including medical writing for content; analysis or interpretation of data. F. Virla: drafting/revision of the manuscript for content, including medical writing for content; analysis or interpretation of data. M. Guandalini: drafting/revision of the manuscript for content, including medical writing for content; major role in the acquisition of data. E. Turano: drafting/revision of the manuscript for content, including medical writing for content; analysis or interpretation of data. F.B. Pizzini: drafting/revision of the manuscript for content, including medical writing for content; major role in the acquisition of data. S. Montemezzi: drafting/revision of the manuscript for content, including medical writing for content; major role in the acquisition of data. B. Bonetti: drafting/revision of the manuscript for content, including medical writing for content; analysis or interpretation of data. O. Howell: drafting/revision of the manuscript for content, including medical writing for content; analysis or interpretation of data. R. Magliozzi: drafting/revision of the manuscript for content, including medical writing for content; major role in the acquisition of data; analysis or interpretation of data. R.S. Nicholas: drafting/revision of the manuscript for content, including medical writing for content; analysis or interpretation of data. A. Scalfari: drafting/revision of the manuscript for content, including medical writing for content; analysis or interpretation of data. C. Granziera: drafting/revision of the manuscript for content, including medical writing for content; analysis or interpretation of data. L. Kappos: drafting/revision of the manuscript for content, including medical writing for content; analysis or interpretation of data. M. Calabrese: drafting/revision of the manuscript for content, including medical writing for content; major role in the acquisition of data; study concept or design; analysis or interpretation of data.

Study Funding

D. Marastoni was supported by the GR-2021-12373041 grant from Italian Ministry of Health. M. Calabrese was supported by the RF-2021-12373319 grant from Italian Ministry of Health. R. Magliozzi was supported by grant from the Italian MS Foundation (FISM 2023/R-Single/038), #NEXTGENERATIONEU (NGEU) and funded by the Ministry of University and Research (MUR), National Recovery and Resilience Plan (NRRP), project MNESYS (PE0000006) - A Multiscale integrated approach to the study of the nervous system in health and disease (DN. 1553 11.10.2022).

Disclosure

The authors report no relevant disclosures. Go to Neurology.org/NN for full disclosures.

Publication History

Received by *Neurology® Neuroimmunology & Neuroinflammation* January 3, 2025. Accepted in final form March 10, 2025. Submitted and externally peer reviewed. The handling editor was Editor Scott S. Zamvil, MD, PhD, FAAN.

References

1. Confavreux C, Vukusic S. Age at disability milestones in multiple sclerosis. *Brain*. 2006;129(Pt 3):595-605. doi:10.1093/brain/awh714
2. Lublin FD, Häring DA, Ganjgahi H, et al. How patients with multiple sclerosis acquire disability. *Brain*. 2022;145(9):3147-3161. doi:10.1093/brain/awac016
3. Scalfari A, Neuhaus A, Degenhardt A, et al. The natural history of multiple sclerosis: a geographically based study 10: relapses and long-term disability. *Brain*. 2010;133(Pt 7):1914-1929. doi:10.1093/brain/awq118
4. Calabrese M, Preziosa P, Scalfari A, et al. Determinants and biomarkers of progression independent of relapses in multiple sclerosis. *Ann Neurol*. 2024;96(1):1-20. doi:10.1002/ana.26913
5. Lassmann H. Pathogenic mechanisms associated with different clinical courses of multiple sclerosis. *Front Immunol*. 2018;9:3116. doi:10.3389/fimmu.2018.03116
6. Steinman L, Zamvil SS. Beginning of the end of two-stage theory purporting that inflammation then degeneration explains pathogenesis of progressive multiple sclerosis. *Curr Opin Neurol*. 2016;29(3):340-344. doi:10.1097/wco.0000000000000317
7. University of California San Francisco MS-EPIC Team, Cree BAC, Hollenbach JA, et al. Silent progression in disease activity-free relapsing multiple sclerosis. *Ann Neurol*.2019;85(5):653-666. doi:10.1002/ana.25463
8. Giovannoni G, Popescu V, Wuerfel J, et al. Smouldering multiple sclerosis: the 'real MS. *Ther Adv Neurol Disord*. 2022;15:17562864211066751. doi:10.1177/17562864211066751
9. Kappos L, Wolinsky JS, Giovannoni G, et al. Contribution of relapse-independent progression vs relapse-associated worsening to overall confirmed disability accumulation in typical relapsing multiple sclerosis in a pooled analysis of 2 randomized clinical trials. *JAMA Neurol*. 2020;77(9):1132-1140. doi:10.1001/jamaneurol.2020.1568
10. Müller J, Cagol A, Lorscheider J, et al. Harmonizing definitions for progression independent of relapse activity in multiple sclerosis: a systematic review. *JAMA Neurol*. 2023;80(11):1232-1245. doi:10.1001/jamaneurol.2023.3331
11. Calabrese M, Magliozzi R, Ciccarelli O, Geurts JJ, Reynolds R, Martin R. Exploring the origins of grey matter damage in multiple sclerosis. *Nat Rev Neurosci*. 2015;16(3):147-158. doi:10.1038/nrn3900
12. Howell OW, Reeves CA, Nicholas R, et al. Meningeal inflammation is widespread and linked to cortical pathology in multiple sclerosis. *Brain*. 2011;134(Pt 9):2755-2771. doi:10.1093/brain/awr182
13. Lucchinetti CF, Popescu BF, Bunyan RF, et al. Inflammatory cortical demyelination in early multiple sclerosis. *N Engl J Med*. 2011;365(23):2188-2197. doi:10.1056/NEJMoa1100648
14. Nicholas R, Magliozzi R, Marastoni D, et al. High levels of perivascular inflammation and active demyelinating lesions at time of death associated with rapidly progressive multiple sclerosis disease course: a retrospective postmortem cohort study. *Ann Neurol*. 2024;95(4):706-719. doi:10.1002/ana.26870
15. Cagol A, Schaedelin S, Barakovic M, et al. Association of brain atrophy with disease progression independent of relapse activity in patients with relapsing multiple sclerosis. *JAMA Neurol*. 2022;79(7):682-692. doi:10.1001/jamaneurol.2022.1025
16. Scalfari A, Romualdi C, Nicholas RS, et al. The cortical damage, early relapses, and onset of the progressive phase in multiple sclerosis. *Neurology*. 2018;90(24):e2107-e2118. doi:10.1212/wnl.0000000000005685
17. Magliozzi R, Howell OW, Nicholas R, et al. Inflammatory intrathecal profiles and cortical damage in multiple sclerosis. *Ann Neurol*. 2018;83(4):739-755. doi:10.1002/ana.25197
18. Magliozzi R, Scalfari A, Pisani AI, et al. The CSF profile linked to cortical damage predicts multiple sclerosis activity. *Ann Neurol*. 2020;88(3):562-573. doi:10.1002/ana.25786
19. Thompson AJ, Banwell BL, Barkhof F, et al. Diagnosis of multiple sclerosis: 2017 revisions of the McDonald criteria. *Lancet Neurol*. 2018;17(2):162-173. doi:10.1016/S1474-4422(17)30470-2
20. Kurtzke JF. Rating neurologic impairment in multiple sclerosis: an expanded disability status scale (EDSS). *Neurology*. 1983;33(11):1444-1452. doi:10.1212/wnl.33.11.1444
21. Poser CM, Paty DW, Scheinberg L, et al. New diagnostic criteria for multiple sclerosis: guidelines for research protocols. *Ann Neurol*. 1983;13(3):227-231. doi:10.1002/ana.410130302
22. Portaccio E, Bellinvia A, Fonderico M, et al. Progression is independent of relapse activity in early multiple sclerosis: a real-life cohort study. *Brain*. 2022;145(8):2796-2805. doi:10.1093/brain/awac111
23. Teunissen CE, Petzold A, Bennett JL, et al. A consensus protocol for the standardization of cerebrospinal fluid collection and biobanking. *Neurology*. 2009;73(22):1914-1922. doi:10.1212/WNL.0b013e3181c47cc2
24. Magon S, Gaetano L, Chakravarty MM, et al. White matter lesion filling improves the accuracy of cortical thickness measurements in multiple sclerosis patients: a longitudinal study. *BMC Neurosci*. 2014;15:106. doi:10.1186/1471-2202-15-106
25. Geurts JJ, Roosendaal SD, Calabrese M, et al. Consensus recommendations for MS cortical lesion scoring using double inversion recovery MRI. *Neurology*. 2011;76(5):418-424. doi:10.1212/WNL.0b013e31820a0cc4
26. STRING. Accessed December 27, 2024. string-db.org/
27. Soroosh P, Doherty TA, So T, et al. Herpesvirus entry mediator (TNFRSF14) regulates the persistence of T helper memory cell populations. *J Exp Med*. 2011;208(4):797-809. doi:10.1084/jem.20101562
28. Tamada K, Shimozaki K, Chapoval AI, et al. Modulation of T-cell-mediated immunity in tumor and graft-versus-host disease models through the LIGHT co-stimulatory pathway. *Nat Med*. 2000;6(3):283-289. doi:10.1038/73136
29. Cheung TC, Steinberg MW, Oborne LM, et al. Unconventional ligand activation of herpesvirus entry mediator signals cell survival. *Proc Natl Acad Sci U S A*. 2009;106(15):6244-6249. doi:10.1073/pnas.0902115106
30. International Multiple Sclerosis Genetics Consortium, Wellcome Trust Case Control Consortium 2, Sawcer S, et al. Genetic risk and a primary role for cell-mediated immune mechanisms in multiple sclerosis. *Nature*. 2011;476(7359):214-219. doi:10.1038/nature10251
31. Malmeström C, Gillett A, Jernås M, et al. Serum levels of LIGHT in MS. *Mult Scler*. 2013;19(7):871-876. doi:10.1177/1352458512463766
32. Anand S, Wang P, Yoshimura K, et al. Essential role of TNF family molecule LIGHT as a cytokine in the pathogenesis of hepatitis. *J Clin Invest*. 2006;116(4):1045-1051. doi:10.1172/jci27083
33. Wang J, Foster A, Chin R, et al. The complementation of lymphotoxin deficiency with LIGHT, a newly discovered TNF family member, for the restoration of secondary lymphoid structure and function. *Eur J Immunol*. 2002;32(7):1969-1979. doi:10.1002/1521-4141(200207)32:7<1969::Aid-immu1969>3.0.Co;2-m
34. Picon C, Jayaraman A, James R, et al. Neuron-specific activation of necroptosis signaling in multiple sclerosis cortical grey matter. *Acta Neuropathol*. 2021;141(4):585-604. doi:10.1007/s00401-021-02274-7
35. Fresegna D, Bullitta S, Musella A, et al. Re-examining the role of TNF in MS pathogenesis and therapy. *Cells*. 2020;9(10):2290. doi:10.3390/cells9102290
36. Magliozzi R, Pezzini F, Pucci M, et al. Changes in cerebrospinal fluid balance of TNF and TNF receptors in naïve multiple sclerosis patients: early involvement in compartmentalised intrathecal inflammation. *Cells*. 2021;10(7):1712. doi:10.3390/cells10071712
37. Bonetti B, Raine CS. Multiple sclerosis: oligodendrocytes display cell death-related molecules in situ but do not undergo apoptosis. *Ann Neurol*. 1997;42(1):74-84. doi:10.1002/ana.410420113
38. Magliozzi R, Howell OW, Durrenberger P, et al. Meningeal inflammation changes the balance of TNF signalling in cortical grey matter in multiple sclerosis. *J Neuroinflammation*. 2019;16(1):259. doi:10.1186/s12974-019-1650-x
39. James RE, Schalks R, Browne E, et al. Persistent elevation of intrathecal pro-inflammatory cytokines leads to multiple sclerosis-like cortical demyelination and neurodegeneration. *Acta Neuropathol Commun*. 2020;8(1):66. doi:10.1186/s40478-020-00938-1
40. Haider L, Prados F, Chung K, et al. Cortical involvement determines impairment 30 years after a clinically isolated syndrome. *Brain*. 2021;144(5):1384-1395. doi:10.1093/brain/awab033
41. Burggraaff J, Liu Y, Prieto JC, et al. Manual and automated tissue segmentation confirm the impact of thalamus atrophy on cognition in multiple sclerosis: a multicenter study. *Neuroimage Clin*. 2021;29:102549. doi:10.1016/j.nicl.2020.102549
42. Calabrese M, Rinaldi F, Grossi P, et al. Basal ganglia and frontal/parietal cortical atrophy is associated with fatigue in relapsing-remitting multiple sclerosis. *Mult Scler*. 2010;16(10):1220-1228. doi:10.1177/1352458510376405
43. Eshaghi A, Marinescu RV, Young AL, et al. Progression of regional grey matter atrophy in multiple sclerosis. *Brain*. 2018;141(6):1665-1677. doi:10.1093/brain/awy088

44. Rocca MA, Mesaros S, Pagani E, Sormani MP, Comi G, Filippi M. Thalamic damage and long-term progression of disability in multiple sclerosis. *Radiology*. 2010;257(2):463-469. doi:10.1148/radiol.10100326
45. Fadda G, Brown RA, Magliozzi R, et al. A surface-in gradient of thalamic damage evolves in pediatric multiple sclerosis. *Ann Neurol*. 2019;85(3):340-351. doi:10.1002/ana.25429
46. Magliozzi R, Fadda G, Brown RA, et al. "Ependymal-in" gradient of thalamic damage in progressive multiple sclerosis. *Ann Neurol*. 2022;92(4):670-685. doi:10.1002/ana.26448
47. Gardner C, Magliozzi R, Durrenberger PF, Howell OW, Rundle J, Reynolds R. Cortical grey matter demyelination can be induced by elevated pro-inflammatory cytokines in the subarachnoid space of MOG-immunized rats. *Brain*. 2013;136(Pt 12):3596-3608. doi:10.1093/brain/awt279
48. Cagol A, Benkert P, Melie-Garcia L, et al. Association of spinal cord atrophy and brain paramagnetic rim lesions with progression independent of relapse activity in people with MS. *Neurology*. 2024;102(1):e207768. doi:10.1212/wnl.0000000000207768
49. Martire MS, Moiola L, Rocca MA, Filippi M, Absinta M. What is the potential of paramagnetic rim lesions as diagnostic indicators in multiple sclerosis?. *Expert Rev Neurother*. 2022;22(10):829-837. doi:10.1080/14737175.2022.2143265
50. Ciccarelli O, Barkhof F, Calabrese M, et al. Using the progression independent of relapse activity framework to unveil the pathobiological foundations of multiple sclerosis. *Neurology*. 2024;103(1):e209444. doi:10.1212/wnl.0000000000209444
51. Prosperini L, Ruggieri S, Haggiag S, Tortorella C, Gasperini C. Disability patterns in multiple sclerosis: a meta-analysis on RAW and PIRA in the real-world context. *Mult Scler*. 2024;30(10):1309-1321. doi:10.1177/13524585241266180